

# An Experimental Study on the Fish Body Flapping Patterns by Using a Biomimetic Robot Fish

Fengran Xie<sup>1</sup>, Zheng Li<sup>2</sup>, *Member, IEEE*, Yang Ding<sup>3</sup>, Yong Zhong<sup>4</sup>, *Member, IEEE*, Ruxu Du<sup>4</sup>

**Abstract**—This paper presents an experimental study on how different body flapping patterns affect the performances of fish cruising. First, a biomimetic robot fish is designed and built as the experimental platform, which mimics the skeleton structure and the muscle arrangement of real fish. Moreover, an improved Central Pattern Generator (CPG) is developed to generate different patterns, which are characterized by four control parameters: (1) the amplitude, (2) the frequency, (3) the time ratio between the beating phase and half cycle, (4) the shape parameter. Then, a number of experiments are conducted to investigate the thrust, the recoil, the cruising speed and the swimming efficiency. Based on the experimental results, following conclusions can be drawn: (1) Fish cruising follows the traveling wave model proposed in Lighthill's Elongated Body Theory. This model offers a balance among the thrust, the recoil and the swimming speed, which results in a high efficiency. (2) The time asymmetry of the body flapping patterns reduces the thrust. (3) The triangular pattern offers the smallest recoil and the cambering sinusoidal pattern gives the largest thrust. These findings provide better understandings on how fish swims and can be used as guidelines for designing the body flapping patterns for robot fish.

**Index Terms**—Robot fish, biomimetics, biologically-inspired robots, body flapping patterns, cruising performances.

## I. INTRODUCTION

It is well known that most fish species swim by coordinately flapping their bodies to generate a traveling wave of increasing amplitude passing from its head toward tail. These fish species are called the Body and/or Caudal Fin (BCF) swimmers, which cover about 85% of the fish species<sup>[1]</sup>. The study of their swimming patterns dates back to last century<sup>[2]</sup>. In late 1960s and early 1970s, Sir Michael James Lighthill presented the

Elongated Body Theory (EBT), in which he gave the traveling wave model<sup>[3]</sup>:

$$y(x, t) = (c_1x + c_2x^2) \sin(kx + \omega t) \quad (1)$$

where,  $y(x, t)$  is the lateral deflection,  $x$  is the displacement along the main axis,  $c_1$  and  $c_2$  are the linear and quadratic wave amplitude envelopes,  $\omega$  is the body wave frequency,  $k$  is the body wave number. This model is subsequently adopted as the norm for fish swimming and robot fish control. However, it is not clear why fish swimming does follow this model. This may be attributed to the fact that real fish is very difficult to control. It is almost impossible to precisely control the individual characteristic parameters of real fish (e.g. the oscillating amplitude, the frequency, the phase lag along the body curve), nor to measure its swimming performances (e.g. the thrust and the torque).

A number of attempts have been made by using simple physical models and/or numerical methods to study the hydrodynamics of fish swimming. When using the simple physical model, fish is usually modelled as a rigid/flexible foil. One general conclusion is that the swimming speed rises with the increase of the amplitude as well as the frequency. An inverse von Karman wake can be found behind the rear of the tail, which is believed to be the cause of this improvement. Kaya *et al.*<sup>[4]</sup> used a gradient based algorithm to optimize the trajectory of a pitching and heaving foil. It showed that the thrust could be improved when using different patterns. Lu *et al.*<sup>[5]</sup> studies the large-amplitude, non-sinusoidal motion of a pitching foil numerically. The results showed that when the pattern was more cambering, the thrust became larger. Hover *et al.*<sup>[6]</sup> studied the thrust and efficiency of a flapping foil under four different flapping profiles, including a harmonic wave, a square wave, a symmetric sawtooth wave and a cosine wave. It was seen that the cosine profile had the best performance for achieving high thrust with a good efficiency. So far, considerable outcomes have been achieved but there are still some limitations: (1) The fish is usually approximated as a rigid/flexible foil in the motion of pitching and/or heaving. The model is too simple to represent the hydrodynamics of real fish. (2) The foil is tethered. Thus, the effect of recoil is ignored. (3) The foil is driven by external motors while fish uses internal muscles. This motivate us to develop an untethered biomimetic robot fish to study fish swimming mechanism.

In the past two decades, a number of robot fishes have been built to serve as a tool for this. For example, Alvarado *et al.*<sup>[7-9]</sup> designed and fabricated a compliant robot fish, and Epps *et al.*<sup>[10]</sup> tested the swimming performances of it, including the swimming speed, Strouhal Number and the thrust. They studied

Manuscript received: April 19, 2019; Revised: August 16, 2019; Accepted: September 7, 2019.

This paper was recommended for publication by Editor Yu Sun upon evaluation of the Associate Editor and Reviewers' comments. This work is supported by the Hong Kong General Research Grants (No. 14212316, No. 14207017, No. 14204417).

<sup>1</sup>Fengran Xie is with the Department of Mechanical and Automation Engineering, the Chinese University of Hong Kong, Hong Kong SAR frxie@mae.cuhk.edu.hk

<sup>2</sup>Zheng Li is with the Department of Surgery and the Chow Yuk Ho Technology Centre for Innovative Medicine, the Chinese University of Hong Kong, Hong Kong SAR lizheng@cuhk.edu.hk

<sup>3</sup>Yang Ding is with the Beijing Computational Science Research Center, Beijing, China dongyang@csrc.ac.cn

<sup>4</sup>Yong Zhong is with S. M. Wu School of Intelligent Engineering, South China University of Technology, Guangzhou 510640, Guangdong, China zhongyong@scut.edu.cn

<sup>4</sup>Ruxu Du is with the S. M. Wu School of Intelligent Engineering, South China University of Technology, Guangzhou 510640, Guangdong, China duruxu@scut.edu.cn

Digital Object Identifier (DOI): see top of this page

how those performance indexes were related to the wake and frequency. In addition, its Strouhal Number was about 0.86. Chen *et al.*<sup>[11]</sup> developed a tensegrity robot fish. The flexible body was made of a series of rigid segments connected with tensegrity joints. The maximum cruising speed of the robot fish was 0.7 Body Length/second (BL/s), and its Strouhal Number was between 0.45 and 0.55. Yu *et al.*<sup>[12,13]</sup> developed a robot dolphin capable of front flipping and back flipping, whose maximum cruising speed was 1.11 BL/s. Its maximum yaw and pitch tuning rate were 31.88 °/s and 303.8 °/s, respectively. Wen *et al.*<sup>[14,15]</sup> developed a self-propel robot fish, whose maximum swimming speed was 0.98 BL/s and its Strouhal Number was 0.375. Marchese *et al.*<sup>[16]</sup> developed a robot fish containing a novel fluidic soft actuation system, and mainly focused on its capability of rapid escape responses. Donati *et al.*<sup>[17]</sup> presented a dummy robot fish consisting of a rigid head and a compliant tail. This robot fish was used to study the collective behavior and electrocommunication in the weakly electric fish. A comprehensive review can be found in the monograph<sup>[18]</sup>.

In biology, Central Pattern Generators (CPGs) refer to neuronal circuits that can produce rhythmic motor patterns without inputs that carry specific timing information<sup>[19]</sup>. Inspired by this mechanism, scientists and researchers have developed CPG control method. It has been applied on many robots, including the robot fish. For example, Alessandro *et al.*<sup>[20]</sup> developed a CPG based amphibious robot fish called BoxyBot, which could perform various motions, like swimming forward, swimming backward, turning, rolling, crawling, ascending/descending. The CPG model had three coupled amplitude-controlled phase oscillators. Similar CPG model was used in the amphibious robot<sup>[21]</sup> and robot fish from Peking University<sup>[22]</sup>. Stefanini<sup>[23]</sup> and Manfredi<sup>[24]</sup> developed a lamprey-like robot. The robot was equipped with several sensors, such as a binocular vision system, and those sensors provided feedback to its CPG controller. It could serve a tool for studying goal-directed locomotion. Wang *et al.*<sup>[25]</sup> combined its CPG model with the dynamic model of a four-joint robot fish. In order to achieve the maximum speed and efficiency, particle swarm optimization (PSO) algorithm was employed to optimize the parameters of the CPG model. Similar work has also been

found in [26]. Zhao *et al.*<sup>[27]</sup> developed a CPG model for a four-joint robot fish, which was capable of three-dimensional locomotion. Coordination among joints were modulated by the connection weights of the CPG model.

Among those studies about fish swimming performance and CPG model, the robot fishes are mainly controlled to follow Lighthill's traveling wave model of (1), which adopts the sinusoidal pattern. Correspondingly, the CPG models usually output a set of coupled sinusoidal signals. Different types of patterns for cruising, such as the pattern with time asymmetry and the non-sinusoidal pattern, and how they affect the swimming performances are rarely reported.

In this paper, we focus on the body flapping motion (the caudal fin flapping motion) of the sub-carangiform swimmers<sup>[28]</sup>, which is characterized by good combination of maneuverability and swimming speed. The objective is to develop an untethered biomimetic robot fish and use it to study how different body flapping patterns affect the performances of fish cruising experimentally. It differs from state-of-the-art in two aspects: 1) Such diverse body flapping patterns applied on an untethered biomimetic robot fish is firstly reported. The flapping pattern is characterized by four parameters: the flapping amplitude ( $M$ ), the flapping frequency ( $f$ ), the time ratio between the beating phase and half cycle ( $R$ ), as well as the waveform shape ( $B$ ) (changing from triangular, to sinusoidal, to cambering sinusoidal). In particular, a full factorial Design of Experiments (DOE) containing  $2^2 \times 3^2 = 36$  tests is carried out to study the stationary thrust. 2) A unique combination of the biomimetic design and an improved CPG model is proposed. On one hand, the design mimics the skeleton structure as well as the muscle arrangement of real fish, and only two motor are needed to perform multimodal swimming, including cruising, turning and ascending/descending. It can approach the hydrodynamic characteristics of real fish, at the same time, simplify the implementation of CPG control. On the other hand, an improved CPG model is presented, which takes the four mentioned parameters as inputs and produce rhythmic flapping patterns.

The rest of this paper is organized as follows. Section II presents the design of the robot fish. Section III gives the improved CPG model and different flapping patterns. Section

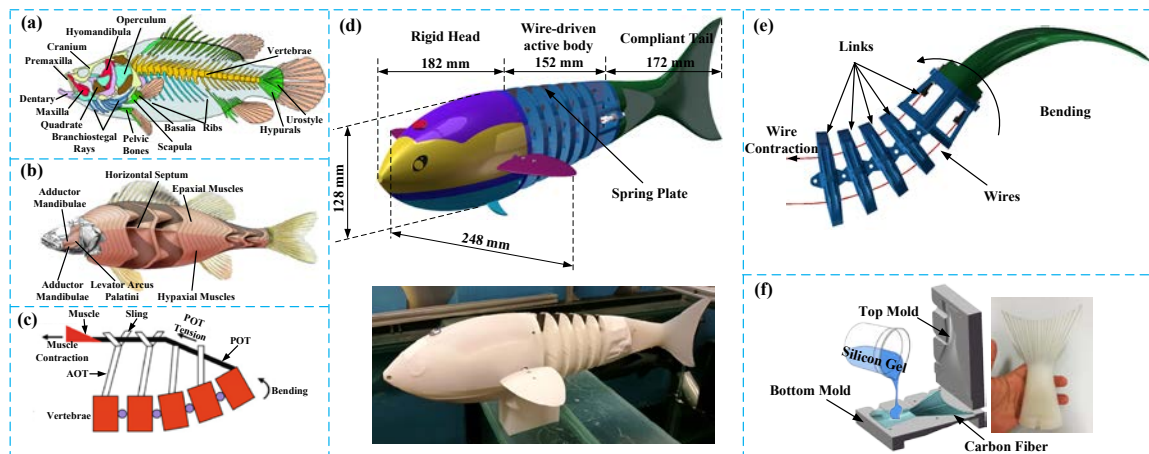


Fig. 1 The design of our robot fish mimics the skeleton and the muscle arrangement of real fish: (a) The skeleton of a fish<sup>[36]</sup>, (b) The muscle arrangement of a fish<sup>[37]</sup>, (c) The backbone bended by the muscle contraction<sup>[38]</sup>, (d) The CAD model and the prototype, (e) The wire-driven propeller of our robot fish follows the real fish, (f) The compliant tail.

IV presents two sets of experiments, the stationary experiment to test the thrust, and the free-swimming experiment to investigate the recoil, the cruising speed and the swimming efficiency. Section V gives detailed discussions. Finally, Section VI contains conclusions and future works.

## II. THE DESIGN OF THE ROBOT FISH

In general, designs of existing robot fishes can be divided into four kinds: the single-joint/multi-joint design (as reported in [12,20,21,25,29]), the design based on smart materials (as reported in [30,31]), the compliant design powered by pneumatics and hydraulics (as reported in [16,32]) and the wire-driven design (as reported in [33-37]). First, the single-joint/multi-joint design uses one link or several links to fit the kinematical model of fish swimming. Its mimicry accuracy depends on the number of the links. More links will increase the mimicry accuracy, while also increase the structure and control complexity. Second, the use of smart materials usually makes the robot fish compact. However, there is a common weakness, i.e., the low energy conversion efficiency. Third, the compliant robot fish can mimic the soft body motion of real fish, and is capable to perform large-amplitude bending, which is favorable for the maneuvering. However, most of them only have one actuator due to the volume limitation, thus, they can only conduct C-Shape motion. Fourth, the wire-driven robot fish has the advantages of employing less actuators, ease of control, etc. But the interactions between the wires of different segments are very complicated. These four designs do not mimic the actuation way of a real fish.

Fig. 1(a) and Fig. 1(b) show the skeleton and the muscle arrangement of a fish. The fish backbone is composed of a number of vertebrae, and the muscle mainly distributes along the backbone. As shown in Fig. 1(c), when the muscle contracts, the backbone will be bended by the posterior oblique tendons (POT), leading to the bending of the fish body. The anterior oblique tendons (AOT) run up from the vertebrae, acting as slings.

This biomimetic robot fish is designed following the actuation way of a real fish. As shown in Fig. 1(d), it consists of a rigid head, a wire-driven active body and a compliant tail. One pair of spring plates with the same stiffness passes through the active body, and the active body is made of several links. They just like the backbone and the vertebrae for the real fish. Then, a pair of wires distributes along the spring plates, which is used to drive the active body. It mimics the muscle arrangement of the real fish (Fig. 1(e)). In biology, it is known that the anterior musculature generates most of the power, and the posterior musculature only transmits force to the tail. By analogy, the anterior muscle is the “motor”, and the tail is the “propeller”<sup>[41]</sup>. Thus, a compliant tail is introduced. The compliant tail is made of silicone gel with carbon fiber reinforcements (Fig. 1(f)). When the active body bends, the compliant tail will lag behind due to the water resistance, resulting in the sub-carangiform swimming. It is seen that the design of the biomimetic robot fish closely follows its counterpart in nature. All the three parts of the robot fish, i.e., the rigid head, the wire-driven active body and the compliant tail, are designed neutrally buoyant.

There are two waterproof servomotors inside the rigid head. One drives the active body and the other drives pectoral fins. All the electrical components, including a microcontroller, batteries, an inertial measurement unit (IMU) and radio frequency (RF) communication modules are mounted inside a customized waterproof box. In comparison to the earlier version<sup>[42]</sup>, this robot fish is larger in volume and more engineering robust. Fluid can flow inside the robot fish to balance the press on the shell. The design specifications of the robot fish are given in Table I.

TABLE I. THE DESIGN SPECIFICATIONS OF THE ROBOT FISH

Items	Specifications
Dimensions (mm)	506(L)×248(W)×128(H)
Length of the rigid head (mm)	182
Length of the active body (mm)	152
Length of the compliant tail (mm)	172
Mass (kg)	1.08
Microcontroller	STM32F103C8
Battery	7.4-VDC 1500-mAH Ni-H battery
Full Duplex Radio Frequency Communication module	E62-433T20S
Servomotors	SAVOX SW-1210S (Active body) HITEC HS-5086WP (Pectoral fins)
Inertial measurement unit (IMU)	MPU 6050

A pair of pectoral fins is used to change the attack angle of the robot fish. By the aid of this, the robot fish can ascend or descend. The pectoral fins are driven by a servomotor through a set of spur gears (number of teeth = 18, module = 0.8, ratio = 1:1). This design is similar with that in [43].

This design largely simplifies the mechanical structure of the robot fish. It has the advantages of employing less actuator, ease of control, and well mimicry of fish locomotion. With only two motors, the robot fish can perform multimodal swimming, such as cruising (Fig. 2(a)), turning (Fig. 2(b)) and ascending/descending (Fig. 2(c)). Please note that even though this design mimics the actuation way of a real fish, it is a bit different from the local contraction of muscles in fish. Indeed, friction is generated when the active body bends. Currently, the servomotor driving the active body is in position control mode. That means, when there is friction generated between the wires and slings, the servomotor will increase its torque corresponding, which overcomes this friction and ensure to the active body can bend to the target position.

The midline curve of the robot fish is mainly formed by the wire-driven active body and the compliant tail. As shown in Fig. 3, one coordinate XOY is set at the first joint,  $d$  is the distance

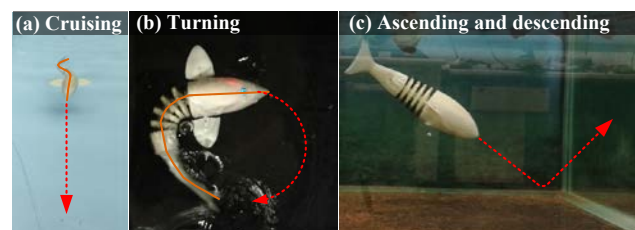


Fig. 2 Multimodal swimming: (a) Cruising, (b) Turning, (c) Ascending and descending.

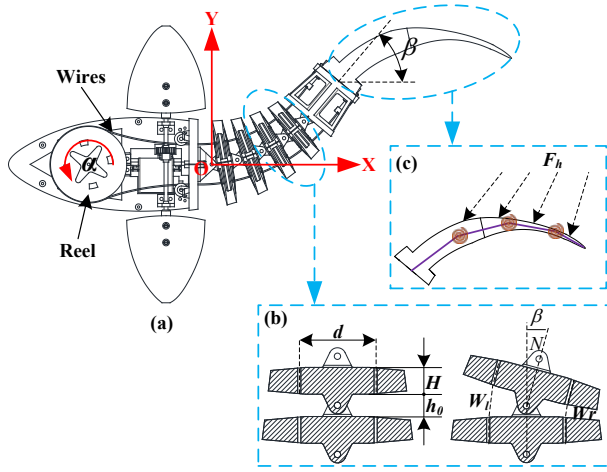


Fig. 3 Illustration of the wire-driven mechanism: (a) Bending state, (b) Bending of one joint, (c) Compliant tail modelled by PRBM theory.

between the two wires inside the link,  $\alpha$  is the rotational angle of the driving motor,  $\beta$  is the bending angle of the wire-driven active body,  $N$  is the number of links,  $h_0$  is the distance between two adjacent links before rotating, and  $H$  is the thickness of one link. The rotational angle of each joint is  $\beta/N$ . Assuming  $\beta/N$  is small, the length changes of the left wire ( $\Delta w_l$ ) and the right wire ( $\Delta w_r$ ) are:

$$|\Delta w_l| = |\Delta w_r| = d \sin\left(\frac{\beta}{2N}\right) \quad (2)$$

Moreover, assuming  $H$  and  $d$  are the same for all links, the relationship between the rotational angle of servomotor,  $\alpha$ , and bending angle of active body,  $\beta$ , is:

$$\beta = 2N \sin^{-1}\left(\frac{\alpha r}{Nd}\right) \quad (3)$$

where  $r$  is the radius of the reel. In our design,  $N=5$ ,  $\alpha \in (-60, +60)$ ,  $d=36$  mm,  $r=33$  mm. The term inside the arcsine function of (3) is small. As a result, (3) can be simplified as:

$$\beta = \frac{2\alpha r}{d} \quad (4)$$

which implies the bending angle of the wire-driven active body follows the pattern of the driving motor.

The position of the  $i^{th}$  joint, which makes the midline curve of the wire-driven active body, can be obtained as follows:

$$\begin{cases} x_i(t) = \sum_{j=1}^i ((H + h_0) \cos(\frac{j\beta}{N})) \\ y_i(t) = \sum_{j=1}^i ((H + h_0) \sin(\frac{j\beta}{N})) \end{cases} \quad (5)$$

The midline curve of the compliant tail is determined by the motion of the active body and the hydrodynamic force ( $F_h$ ). By using the Pseudo-Rigid-Body Model (PRBM)<sup>[44]</sup>, the compliant tail can be modeled as rigid links connected serially through torsional springs. Moreover, the hydrodynamic force ( $F_h$ ) can be calculated by using Lighthill's Large-amplitude Elongated-body Theory (LAEBT)<sup>[45,46]</sup>. Details about the wire-driven mechanism and compliant tail can be found in [42].

### III. AN IMPROVED CPG MODEL AND DIFFERENT FLAPPING PATTERNS

To realize the flexible fishlike locomotion, the Central Pattern Generator (CPG) method is adopted to control the biomimetic robot fish. In comparison with the sinusoidal-based method, CPG facilitates online modification of parameters and coordination among joints<sup>[47,48]</sup>. In this section, an improved CPG model is developed to generate patterns with different amplitudes, frequencies, time ratios and shapes.

As shown in Fig. 4, one cycle is divided into 4 phases: Phase I – beating right, Phase II – restoring, Phase III – beating left, Phase IV – restoring. The time durations of these four phases are  $t_I$ ,  $t_{II}$ ,  $t_{III}$ ,  $t_{IV}$ , respectively. Phase I and Phase III are called the beating phase, while Phase II and Phase IV are called the restoring phase. In cruising, the two half cycles are symmetrical. That means,  $t_I = t_{III}$  and  $t_{II} = t_{IV}$ .

We starts from the CPG model persented in [25], which is based on Hopf oscillator. Note that our robot fish only needs one servomotor for cruising, the coupling terms in the model are eliminated. Thus, this CPG model is given as:

$$\dot{u} = k_a(1 - u^2 - v^2)u - 2\pi f_a v \quad (6)$$

$$\dot{v} = k_a(1 - u^2 - v^2)v + 2\pi f_a u \quad (7)$$

where  $u$  and  $v$  are the state variables,  $f_a$  is the oscillation frequency,  $k_a$  is a positive constant which determines the converging speeds of  $u$  and  $v$ . When the oscillator is in a steady state,  $u$  and  $v$  are both sinusoidal signals with a phase shift

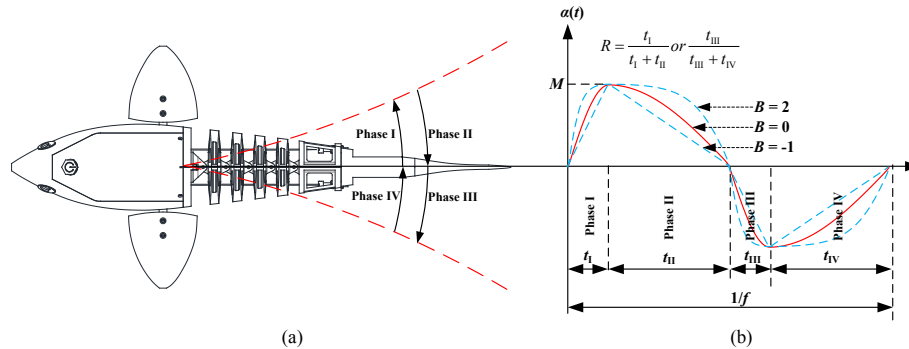


Fig. 4 Illustration of the flapping patterns: (a) Four phases of one cycle, (b) Control parameters and the pattern

between them (amplitude = 1, frequency =  $f_a$ , offset = 0). In this paper,  $u$  is chosen as the output of oscillator, and  $v$  is an intermediate variable.

Then, an improvement is made to the oscillation frequency  $f_a$ , which is given as:

$$f_a = f_1 + (f_2 - f_1)S_\tau(uv) \quad (8)$$

$$f_1 = \frac{f}{2R} \quad (9)$$

$$f_2 = \frac{f}{2(1-R)} \quad (10)$$

where  $S_\tau(uv) = 1/(1 + e^{-\tau uv})$  is a sigmoid function. It switches  $f_a$  adaptively between  $f_1$  and  $f_2$  based on the multiplication of state variables  $u$  and  $v$ .  $f$  is the new control parameter modulating the oscillation frequency.  $0 < R < 1$  is the ratio between the time duration of a beating phase and half cycle, which is defined as:

$$R = \frac{t_I}{t_I + t_{II}} \text{ or } \frac{t_{III}}{t_{III} + t_{IV}} \quad (11)$$

When  $R = 0.5$ , the time durations of Phase I (III) and Phase II (IV) are the same. There is no time asymmetry. When  $R \neq 0.5$ , the time durations of Phase I (III) and Phase II (IV) are not the same. There exists time asymmetry.

In addition, the output of the oscillator,  $u$ , is further processed by following equations:

$$\ddot{b} = k_b(0.25k_b(B - b) - \dot{b}) \quad (12)$$

$$\ddot{m} = k_m(0.25k_m(M - m) - \dot{m}) \quad (13)$$

$$\alpha(t) = \begin{cases} \frac{m \cdot \tanh(bu)}{\tanh(b)}, & b > 0 \\ mu, & b = 0 \\ \frac{m \cdot \sin^{-1}(-bu)}{\sin^{-1}(-b)}, & -1 \leq b < 0 \end{cases} \quad (14)$$

where  $\alpha(t)$  is the output of the CPG model, which is used to control the servomotor driving the active body.  $B \geq -1$  is the shape control parameter, which changes the shape of  $\alpha(t)$  from triangular, to sinusoidal, to cambering sinusoidal.  $M > 0$  is the amplitude control parameter.  $b$  is the state of the shape parameter.  $m$  is the state of the amplitude.  $k_b$  and  $k_m$  are positive constants. It is seen that (12) and (13) are second-order differential equations in critical damping. That means when  $B$  and  $M$  change, their states,  $b$  and  $m$ , will track them correspondingly. The conversing speed can be modulated by the positive constant  $k_b$  and  $k_m$ . Particularly, when  $B = -1$ , the output  $\alpha(t)$  is triangular; when  $B = 0$ ,  $\alpha(t)$  is sinusoidal; when  $B > 0$ ,  $\alpha(t)$  is cambering sinusoidal.

Finally, the control command of the improved CPG model is defined as  $(M, f, R, B)$ , where  $M$  is the control parameter of amplitude,  $f$  is the control parameter of frequency,  $R$  is the control parameter of time ratio between beating phase and half cycle, and  $B$  is the control parameter of shape. Fig. 4(b) shows

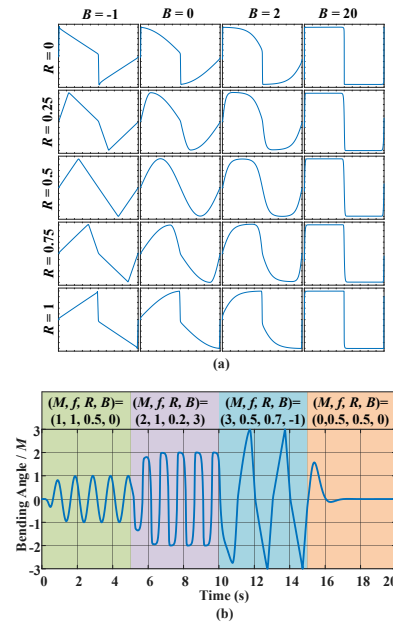


Fig. 5 The output of the improved CPG model: (a) Under different combinations of  $R$  and  $B$ , (b) Transitions among different patterns.

how these four control parameters are related to the output of the CPG model.

In comparison to other existing CPG models used in robot fish, this improved CPG model can produce more diverse patterns. The pattern can have different amplitudes, frequencies, time asymmetries, and shapes (changing from triangular to sinusoidal, to cambering sinusoidal). As an example, Fig. 5(a) shows  $\alpha(t)$  under different combinations of  $R$  and  $B$ . Please note that some patterns with very sharp discontinuities are not realizable for electro-mechanical actuators, such as a servomotor. When applying the CPG model, the commanded pattern needs to be ensured in the actuator's capacity. In addition, CPG also facilitates the transitions among different patterns. Another simulation example is shown in Fig. 5(b), where  $k_a = 10$ ,  $k_b = k_m = 7$ ,  $\tau = 50$ . When the control command  $(M, f, R, B)$  changes as:  $(1, 1, 0.5, 0) \rightarrow (2, 1, 0.2, 3) \rightarrow (3, 0.5, 0.7, -1) \rightarrow (0.5, 0.5, 0.5, 0)$ . It is seen that the transitions among these four patterns are smooth.

#### IV. EXPERIMENTAL RESULTS

The improved CPG model proposed in Section III is implemented onto the untethered biomimetic robot fish to study how different body flapping patterns affect the performances of fish cruising. A large number of experiments have been conducted. Two sets of experiments are shown: the stationary experiment to test the thrust, and the free-swimming experiment to investigate the recoil, the cruising speed and the swimming efficiency.

##### A. The Stationary Experiment

This set of experiments is designed to measure the thrust under various body flapping patterns when the robot fish is mounted. The experimental station is shown in Fig. 6. The robot fish is mounted on a bracket. A computer is equipped with a data acquisition board (Model: USB-6001) to receive the force data



Fig. 6 The setup for the stationary experiment

obtained by a load cell (Model: HSTL-BLSM). Through a Radio Frequency communication module (Model: APC220), the computer sends the control commands to the robot fish and receives data back. One joy sticker is used to remotely control the robot fish. The computer program is written through LabVIEW®.

In this Design of Experiments (DOE),  $M$  and  $f$  are two-level factors while  $R$  and  $B$  are three-level factors. The levels and the corresponding values are demonstrated in Table II. Therefore, a full factorial DOE of totally  $2^2 \times 3^2 = 36$  tests is conducted. In each test, the robot fish is controlled to flap 10 times. Fig. 7 shows the experimental results, from which following observations can be made:

TABLE II. THE LEVELS OF THE CONTROL PARAMETERS

Level	$M$	$f$	$R$	$B$
Low	10	0.5	0.25	-1 (Triangular)
Mid	-	-	0.5	0 (Sinusoidal)
High	15	2	0.75	2 (Cambering Sinusoidal)

- (1) The stationary thrust grows with the increase of the amplitude and the frequency (Fig. 7(a) and Fig. 7(b)).
- (2) When the frequency is low, the time ratio does not influence the thrust so much. However, when the frequency is high, the pattern with  $R = \text{Mid}$  (0.5) achieves the largest thrust (Fig. 7(c)). This implies the time asymmetry deteriorates the thrust generation.
- (3) The thrust grows with the increase of the shape parameter  $B$  (Fig. 7(d)). That means the cambering effect increases the thrust generation. The cambering sinusoidal pattern achieves the largest thrust, followed by the sinusoidal pattern and the triangular pattern.

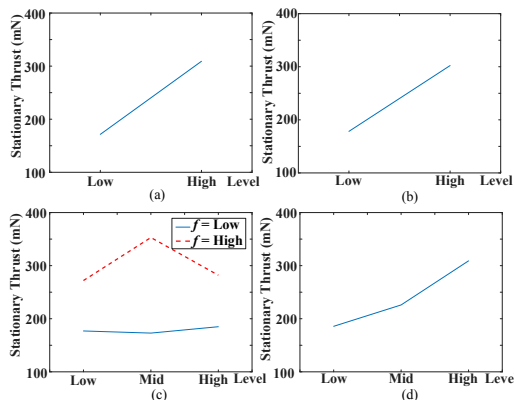


Fig. 7 The stationary thrust under different levels of control parameters: (a) The amplitude, (b) The frequency, (c) The time ratio, (d) The shape parameter.

## B. The Free-swimming Experiment

According to the data from the stationary experiment, the cambering sinusoidal pattern has the largest thrust. However, the sinusoidal pattern is adopted in the traveling wave model of (1). Is the fish not smart enough to choose the pattern that has larger thrust? Following this question, this set of experiments is designed to test other cruising performances (the recoil, the swimming speed, the swimming efficiency) under three typical body flapping patterns (the triangular pattern, the sinusoidal pattern, the cambering sinusoidal pattern). In contrast to the stationary experiment, the robot fish will swim freely. Moreover, to produce larger thrust,  $M$  is set to High,  $f$  is set to High, and  $R$  is set to Mid. Each pattern is repeated 5 times.

When the fish swims, its head may swing from side to side, which is termed as recoil. Recoil affects the performances of fish cruising. Actually, recoil refers to the yaw motion. In this experiment, the yaw angle and yaw angular velocity are recorded by an onboard IMU. The instant yaw angle and yaw angular velocity are demonstrated in Fig. 8. It is seen that the instant yaw angle and yaw angular velocity of the sinusoidal pattern also change sinusoidally in the same frequency of the control command. However, those of the triangular and cambering sinusoidal patterns have small glitches or jumps, which make them not as smooth as the sinusoidal pattern. The mean yaw angle, peak-to-peak yaw angle, mean yaw angular velocity and peak-to-peak yaw angular velocity are shown in Table III. It is found that the triangular pattern has the smallest recoil, followed by the sinusoidal pattern and the cambering sinusoidal pattern. Particularly, the cambering sinusoidal pattern has the peak-to-peak yaw angular velocity up to  $598^\circ/\text{s}$ .

From Table III, it is seen that the cruising speed under the sinusoidal pattern is comparable to that under the cambering pattern, up to 0.83 BL/s. And the cruising speed under the triangular pattern is the lowest, only 0.69 BL/s.

In the aquatic animal's locomotion, the Strouhal Number,  $SN$ , is defined as<sup>[49]</sup>:

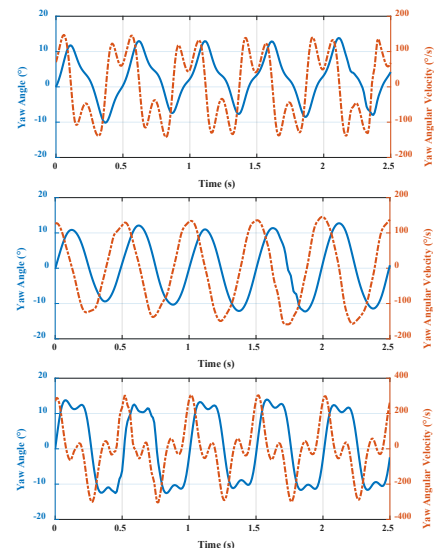


Fig. 8 The yaw angle and yaw angular velocity: (a) Triangular, (b) Sinusoidal, (c) Cambering sinusoidal.

TABLE III. EXPERIMENTAL RESULTS OF THE RECOIL, THE SWIMMING SPEED AND THE SWIMMING EFFICIENCY

Body Flapping Pattern	Recoil				Swimming Speed	Swimming Efficiency
	Average yaw angle (°)	Peak-to-peak yaw angle (°)	Average yaw angular velocity (°/s)	Peak-to-peak yaw angular velocity (°/s)	Mean Swimming Speed (BL/s) *	Strouhal Number
Triangular	5.6	21.2	87	279	0.69	0.97
Sinusoidal	7.3	22.7	91	280	0.84	0.69
Cambering sinusoidal	9.5	25.1	109	598	0.83	0.8

\* BL/S stands for Body Length / Second

$$SN = \frac{fA_{p-p}}{U} \quad (15)$$

where  $f$  is the frequency,  $A_{p-p}$  is the peak-to-peak amplitude at the tail end,  $U$  is the cruising speed. Most of the aquatic animals have their Strouhal Numbers falling in the narrow range between 0.2 and 0.4, and the efficiency is high within this range<sup>[50,51]</sup>. Thus, the Strouhal Number is used to qualitatively indicate the efficiency of fish swimming. The Strouhal Numbers of the robot fish are also shown in Table III. It is seen that the Strouhal Number under the sinusoidal pattern is the closest to the narrow range (0.2~0.4), followed by the cambering sinusoidal pattern and the triangular pattern. Thus, it might be said that the swimming efficiency under the sinusoidal pattern is the highest and that under the triangular is the lowest. The cambering sinusoidal is in the middle.

## V. DISCUSSIONS

Fish cruising follows Lighthill's traveling wave model, which has two characteristics: 1) No time asymmetry; 2) The sinusoidal pattern is adopted. Why nature chooses this model can be explained as follows:

(a) The introduction of the asymmetrical pattern deteriorates the thrust generation. This is attributed to the fact that the asymmetrical pattern generates large recoil and thus, is not favored. It is interesting to note that when turning, fish does use asymmetrical pattern. It bends quickly to the limit position and restores slowly, which leads to a large torque for turning.

(b) The cambering sinusoidal pattern increases the thrust as well as the recoil. As a result, it gives an increasing speed but decreasing efficiency. This is because a significant portion of the energy is consumed to overcome the water resistance caused by the recoil.

(c) The triangular pattern decreases the recoil but also decreases the speed. This is because a smaller amount of water is propelled and hence, the thrust is small.

(d) Table IV summarizes the experimental results. From the table, it is seen that nature favors the sinusoidal pattern because it balances the thrust, the recoil, and the swimming speed, which, in return, gives the highest swimming efficiency. In practical applications, one could choose specific pattern based on the demand. When the acceleration is important, like fast start, the cambering sinusoidal pattern is preferred. When small recoil is needed, like staying with a group, the triangular pattern is recommended. For long-distance swimming, it is better to use the sinusoidal pattern.

TABLE IV. SUMMARY OF DIFFERENT PATTERNS

Body Flapping Pattern	Stationary thrust	Recoil	Cruising speed	Swimming efficiency
Triangular	Small	Small	Slow	Low
Sinusoidal	Middle	Middle	Fastest	High
Cambering sinusoidal	Large	Large	Fast	Middle

## VI. CONCLUSIONS AND FUTURE WORKS

This paper presents a systematic experimental study on how different patterns affect the cruising performances. Based on the discussions above, following conclusions can be made:

- (1) The presented untethered biomimetic robot fish is effective to study the fish swimming patterns, because: (a) In comparison with a real fish, the biomimetic robot fish is controllable, and the performances are easier to measure. (b) Compared with other robot fishes, it adopts a rigid-compliant coupled design consisting of a rigid head, a wire-driven active body and a compliant tail. This design follows the skeleton structure, the muscle arrangement and the power generation principle of the real fish, thus, it can better resemble the behaviors of its counterpart in nature. In the control side, the improved CPG model can generate more diverse patterns with four parameters controlling the amplitude, the frequency, the time ratio and the shape.
- (2) Nature favors the Lighthill's traveling wave model for cruising. This is because it provides a balance among the thrust, the recoil and the swimming speed, which leads to the high swimming efficiency.
- (3) The triangular pattern gives the smallest recoil, and the cambering sinusoidal pattern gives the largest thrust. The time asymmetry of the body flapping pattern deteriorates the thrust generation.

In the future, various issues need to be investigated, including how the fish turns, the dynamics and hydrodynamics of our biomimetic robot fish, as well as the functions of pectoral fins.

## ACKNOWLEDGMENT

The authors would like to thank Mr. Allan Mok Wai Kit for his help in conducting the experiments.

## REFERENCES

- [1] T. Fukuda, F. Chen and Q. Shi, *Bio-Inspired Robotics*. Basel, Switzerland: Applied Sciences, 2018.
- [2] J. Gray, "Studies in animal locomotion: I. The movement of fish with

- special reference to the eel," *Journal of experimental biology*, vol. 10, no. 1, pp. 88-104, 1933.
- [3] M.J. Lighthill, *Mathematical Biofluidynamics*. Philadelphia, USA: SIAM Society for Industrial and Applied Mathematics, 1975.
- [4] M. Kaya and I.H. Tuncer, "Nonsinusoidal path optimization of a flapping airfoil," *AIAA journal*, vol. 45, no. 8, pp. 2075-2082, 2007.
- [5] K. Lu, Y.H. Xie and D. Zhang, "Numerical study of large amplitude, nonsinusoidal motion and camber effects on pitching airfoil propulsion," *Journal of Fluids and Structures*, vol. 36, pp. 184-194, 2013.
- [6] F.S. Hover, Ø. Haugsdal and M.S. Triantafyllou, "Effect of angle of attack profiles in flapping foil propulsion," *Journal of Fluids and Structures*, vol. 19, no. 1, pp. 37-47, 2004.
- [7] PV y Alvarado, "Design of biomimetic compliant devices for locomotion in liquid environments," Ph.D. dissertation, Massachusetts Institute of Technology, 2007.
- [8] PV y Alvarado and K. Youcef-Toumi, "Design of machines with compliant bodies for biomimetic locomotion in liquid environments," *ASME Journal of dynamic systems, measurement, and control*, vol. 128, no. 1, pp. 3-13, 2006.
- [9] PV y Alvarado and K. Youcef-Toumi, "Modeling and Design Methodology of an Efficient Underwater Propulsion System," in *Proc. LASTED International Conference Robotics and Applications*, 2003, pp. 161-166.
- [10] B.P. Epps, PV y Alvarado, K. Youcef-Toumi and A.H. Techet, "Swimming performance of a biomimetic compliant fish-like robot," *Experiments in Fluids*, vol. 47, no. 6, pp. 927, Epps2009, 2009.
- [11] B. Chen and H. Jiang, "Swimming Performance of a Tensegrity Robotic Fish," *Soft Robotics*, vol. 6, no. 4, pp. 520-531, 2019.
- [12] J. Yu, Z. Su, M. Wang, M. Tan and J. Zhang, "Control of Yaw and Pitch Maneuvers of a Multilink Dolphin Robot," *IEEE Transactions on Robotics*, vol. 28, no. 2, pp. 318-329, 2012.
- [13] J. Yu, M. Wang, M. Tan and J. Zhang, "Three-Dimensional Swimming," *IEEE Robotics & Automation Magazine*, vol. 18, no. 4, pp. 47-58, 2011.
- [14] L. Wen, G. Wu and J. Li, "Hydrodynamic experimental investigation on efficient swimming of robotic fish using self-propelled method," *International Journal of Offshore and Polar Engineering*, vol. 20, no. 03, 2010.
- [15] L. Wen, T. Wang, G. Wu and J. Liang, "Quantitative thrust efficiency of a self-propulsive robotic fish: Experimental method and hydrodynamic investigation," *IEEE/ASME Transactions on Mechatronics*, vol. 18, no. 3, pp. 1027-1038, 2013.
- [16] A.D. Marchese, C.D. Onal and D. Rus, "Autonomous soft robotic fish capable of escape maneuvers using fluidic elastomer actuators," *Soft Robotics*, vol. 1, no. 1, pp. 75-87, 2014.
- [17] E. Donati, M. Worm, S. Mintchev, M. Van Der Wiel, G. Benelli and G. Von Der Emde, *et al.*, "Investigation of collective behaviour and electrocommunication in the weakly electric fish, *Mormyrus rume*, through a biomimetic robotic dummy fish," *Bioinspiration & biomimetics*, vol. 11, no. 6, pp. 66009, 2016.
- [18] R. Du, Z. Li, K. Youcef-Toumi and PV y Alvarado, *Robot fish: Bio-Inspired Fishlike Underwater Robots*. New York, USA: Springer, 2015.
- [19] E. Marder and D. Bucher, "Central pattern generators and the control of rhythmic movements," *Current biology*, vol. 11, no. 23, pp. R986-R996, 2001.
- [20] A. Crespi, D. Lachat, A. Pasquier and A.J. Ijspeert, "Controlling swimming and crawling in a fish robot using a central pattern generator," *Autonomous Robots*, vol. 25, no. 1-2, pp. 3-13, 2008.
- [21] J. Yu, R. Ding, Q. Yang, M. Tan and J. Zhang, "Amphibious Pattern Design of a Robotic Fish with Wheel-propeller-fin Mechanisms," *Journal of Field Robotics*, vol. 30, no. 5, pp. 702-716, 2013.
- [22] J. Yu, C. Wang and G. Xie, "Coordination of Multiple Robotic Fish With Applications to Underwater Robot Competition," *IEEE Transactions on Industrial Electronics*, vol. 63, no. 2, pp. 1280-1288, 2016.
- [23] C. Stefanini, S. Orofino, L. Manfredi, S. Mintchev, S. Marrazza and T. Assaf, *et al.*, "A novel autonomous, bioinspired swimming robot developed by neuroscientists and bioengineers," *Bioinspiration & biomimetics*, vol. 7, no. 2, pp. 25001, 2012.
- [24] L. Manfredi, T. Assaf, S. Mintchev, S. Marrazza, L. Capantini and S. Orofino, *et al.*, "A bioinspired autonomous swimming robot as a tool for studying goal-directed locomotion," *Biological cybernetics*, vol. 107, no. 5, pp. 513-527, 2013.
- [25] M. Wang, H. Dong, X. Li, Y. Zhang and J. Yu, "Control and Optimization of a Bionic Robotic Fish Through a Combination of CPG model and PSO," *Neurocomputing*, vol. 337, pp. 144-152, 2019.
- [26] J. Yu, Z. Wu, M. Wang and M. Tan, "CPG network optimization for a biomimetic robotic fish via PSO," *IEEE Transactions on Neural Networks and Learning Systems*, vol. 27, no. 9, pp. 1962-1968, 2016.
- [27] W. Zhao, Y. Hu, L. Zhang and L. Wang, "Design and CPG-based control of biomimetic robotic fish," *IET Control Theory & Applications*, vol. 3, no. 3, pp. 281-293, 2009.
- [28] M. Sfakiotakis, D.M. Lane and J.B.C. Davies, "Review of fish swimming modes for aquatic locomotion," *IEEE Journal of Oceanic Engineering*, vol. 24, no. 2, pp. 237-252, 1999.
- [29] J. Liu and H. Hu, "Biological inspiration: from carangiform fish to multi-joint robotic fish," *Journal of bionic engineering*, vol. 7, no. 1, pp. 35-48, 2010.
- [30] Z. Chen, S. Shatara and X. Tan, "Modeling of Biomimetic Robotic Fish Propelled by An Ionic Polymer - Metal Composite Caudal Fin," *IEEE/ASME Transactions on Mechatronics*, vol. 15, no. 3, pp. 448-459, 2010.
- [31] S. Zhang, B. Liu, L. Wang, Q. Yan, K.H. Low and J. Yang, "Design and Implementation of a Lightweight Bioinspired Pectoral Fin Driven by SMA," *IEEE/ASME Transactions on Mechatronics*, vol. 19, no. 6, pp. 1773-1785, 2014.
- [32] R.K. Katzschmann, J. DelPreto, R. MacCurdy and D. Rus, "Exploration of underwater life with an acoustically controlled soft robotic fish," *Science Robotics*, vol. 16, no. 3, pp. r3449, 2018.
- [33] Z. Li and R. Du, "Design and analysis of a biomimetic wire-driven flapping propeller," in *Proc. 4th IEEE RAS & EMBS International Conference on Biomedical Robotics and Biomechanics (BioRob)*, IEEE, 2012, pp. 276-281.
- [34] Z. Li, W. Gao, R. Du and B. Liao, "Design and analysis of a wire-driven robot tadpole," in *Proc. ASME 2012 International Mechanical Engineering Congress and Exposition*, ASME, 2012, pp. 297-303.
- [35] Z. Li, R. Du, Y. Zhang and H. Li, "Robot fish with novel wire-driven continuum flapping propulsor," *Applied Mechanics and Materials*, vol. 300, pp. 510-514, 2013.
- [36] B. Liao, Z. Li and R. Du, "Robot tadpole with a novel biomimetic wire-driven propulsor," in *Proc. 2012 IEEE International Conference on Robotics and Biomimetics (ROBIO)*, IEEE, 2012, pp. 557-562.
- [37] B. Liao, Z. Li and R. Du, "Robot fish with a novel biomimetic wire-driven flapping propulsor," *Advanced Robotics*, vol. 28, no. 5, pp. 339-349, 2014.
- [38] <https://www.earthlife.net/fish/skeleton.html>
- [39] [https://www.animaldiversity.org/collections/contributors/Grzimek\\_fish/structu\\_re\\_function/v04\\_id131\\_con\\_axialmu/](https://www.animaldiversity.org/collections/contributors/Grzimek_fish/structu_re_function/v04_id131_con_axialmu/)
- [40] R.M. Alexander, *Elastic mechanisms in animal movement*. Cambridge: Cambridge University Press, 1988.
- [41] D.W. Linzey, *Vertebrate biology*: JHU Press, 2012.
- [42] Y. Zhong, Z. Li and R. Du, "A Novel Robot Fish with Wire-driven Active Body and Compliant Tail," *IEEE/ASME Transactions on Mechatronics*, vol. PP, no. 99, pp. 1, 2017.
- [43] J. Yu, R. Ding, Q. Yang, M. Tan, W. Wang and J. Zhang, "On a Bio-inspired Amphibious Robot Capable of Multimodal Motion," *IEEE/ASME Transactions on Mechatronics*, vol. 17, no. 5, pp. 847-856, 2012.
- [44] L.L. Howell, *Compliant Mechanisms*. Canada: John Wiley & Sons, 2001.
- [45] M.J. Lighthill, "Large-amplitude elongated-body theory of fish locomotion," *Proceedings of the Royal Society of London. Series B, Biological Sciences*, pp. 125-138, 1971.
- [46] J. Wang, P.K. McKinley and X. Tan, "Dynamic modeling of robotic fish with a base-actuated flexible tail," *ASME Journal of dynamic systems, measurement, and control*, vol. 137, no. 1, pp. 11004, 2015.
- [47] Z. Bing, L. Cheng, K. Huang, M. Zhou and A. Knoll, "CPG-based control of smooth transition for body shape and locomotion speed of a snake-like robot," in *Proc. 2017 IEEE International Conference on Robotics and Automation (ICRA)*, 2017, pp. 4146-4153.
- [48] T. Wang, Y. Hu and J. Liang, "Learning to swim: a dynamical systems approach to mimicking fish swimming with CPG," *Robotica*, vol. 31, no. 3, pp. 361-369, 2013.
- [49] R.M. Alexander, *Principles of animal locomotion*. New Jersey, USA: Princeton University Press, 2003.
- [50] M.S. Triantafyllou, G.S. Triantafyllou and R. Gopalkrishnan, "Wake mechanics for thrust generation in oscillating foils," *Physics of Fluids A: Fluid Dynamics*, vol. 3, no. 12, pp. 2835-2837, 1991.
- [51] M.S. Triantafyllou, G.S. Triantafyllou and D. Yue, "Hydrodynamics of fishlike swimming," *Annual Review of Fluid Mechanics*, vol. 32, no. 1, pp. 33-53, 2000.